Energy Advances

ROYAL SOCIETY OF CHEMISTRY

PAPER

View Article Online
View Journal | View Issue

Cite this: *Energy Adv.*, 2023, 2, 1022

Hydrogen and oxygen evolution reactions on single atom catalysts stabilized by a covalent organic framework†

Ilaria Barlocco, Giovanni Di Liberto * and Gianfranco Pacchioni

Received 13th April 2023,
Accepted 9th May 2023

DOI: 10.1039/d3ya00162h

rsc.li/energy-advances

Single Atom Catalysts (SACs) bridge homo- and heterogenous catalysis and are promising for several chemical processes of interest, including water splitting. SACs can form reaction adducts that do not likely form on conventional metal catalysts. Besides the typical supporting matrices made by carbon-based materials, Covalent Organic Frameworks (COFs) are gaining attention because of the possibility to design the hosting cavity to stably bind the active metal site. We performed a density functional theory (DFT) study of a set of SACs made by transition metal atoms embedded in a recently synthesized COF material. We explored their reactivity in Hydrogen and Oxygen Evolution Reactions (HER and OER, respectively). SACs@COF can form several intermediates with no counterpart on the classical metal electrodes, with important implications on the reaction mechanism. The results are useful for the design of novel catalytic materials and for the identification of interpretative/predictive activity descriptors.

1. Introduction

Single atom catalysis is a relatively new frontier bridging the two worlds of homogeneous and heterogenous catalysts.[1–6] In a single atom catalyst (SAC), transition metal (TM) atoms are dispersed atomically in a solid matrix. The atomic dispersion allows in principle maximization of the active phase, and tailoring of the activity by playing with the local environment.[7–9] Both aspects are of paramount importance for the development of a new generation of catalytic materials with high activity and limited amounts of precious materials.

SACs can be considered analogs of coordination chemistry compounds,[8,10,11] and the TM atom embedded in a solid matrix can bind and activate molecular species. The reactivity is sensitive to the local coordination and to the nature of the ligand atoms of the support.[7,8,12] This hallmark of SACs has intriguing potential implications in catalysis, since the reactivity can be substantially different from that of conventional catalysts based on extended metal surfaces.[13,14] Typical supports of SACs are 2D materials such as graphene, nitrogen-doped graphene, carbon nitride, MoS_2 and MXenes.[2,15–25]

A relatively novel family of supports is that of Covalent Organic Frameworks (COF), porous crystalline polymers.[26–28] COFs are periodic frameworks of organic building blocks held together by covalent interactions. They are characterized by cavities of tunable size depending on the nature of the composing blocks.[29] The possibility to rationally design the cavity size and its symmetry allows one to engineer the local environment with atomistic precision. The cavities can be used to stabilize atomically dispersed metal species. Therefore, COFs are excellent templates for SACs. Several examples of COFs used to stabilize TM atoms have been reported in the literature. For instance, Meng *et al.* prepared a two-dimensional COF with optimal sensing response to several gas phase molecules.[30] A similar framework was synthetized by Yue *et al.* and successfully applied for CO_2 reduction in aqueous media.[31] A detailed review of 2D COFs was published recently by Guan *et al.*[32] 2D COFs have also stimulated several computational screening studies.[33,34] A recent example of a supporting matrix for SACs is a COF material shown in Fig. 1; this was obtained through the combination of metallophthalocyanine and pyrazine.[34,35] The crystalline structure is characterized by a pore able to host a TM atom coordinated by four in plane nitrogen atoms, Fig. 1. This arrangement is reminiscent of that of porphyrins and nitrogen-doped graphene,[7,36] and therefore it is expected to be able to strongly bind the active phase, thus preventing sintering. This system has been successfully synthetized and applied for CO_2 reduction.[35] A recent screening study was performed aiming at unveiling promising SACs for N_2 electroreduction.[34]

In this work we performed a systematic computational study of SACs made by a series of 3d, 4d, and 5d TM atoms (Fig. 1) and their reactivity in Hydrogen Evolution (HER) and Oxygen Evolution (OER) reactions, the two fundamental chemical

Dipartimento di Scienza dei Materiali, Università degli Studi di Milano Bicocca, Via R. Cozzi 55 (20125), Milano, Italy. E-mail: giovanni.diliberto@unimib.it

† Electronic supplementary information (ESI) available. See DOI: https://doi.org/10.1039/d3ya00162h

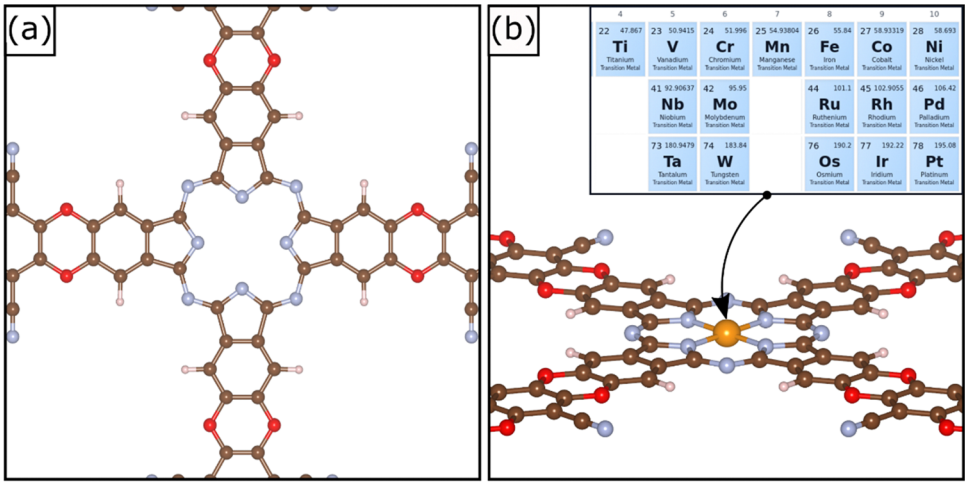

Fig. 1 (a) Top view of the selected COF and (b) example of the TM@COF structure. Inset: TMs selected for this study. Oxygen (red), carbon (brown), nitrogen (light blue) and hydrogen (white). The generic metal atom in (b) is indicated in orange.

processes of the electrochemical water splitting. Given the steadily growing number of computational studies on SACs it is important to underline the main novelty of the present study. We will show that the chemistry of SACs supported on COF is complex and reminiscent of coordination chemistry, since several intermediates can form in analogy with previous studies on carbon-based materials.[13,14,37,38] These intermediates differ from those usually found on metal electrodes, and therefore are classified as ''unconventional''. Including also the unconventional intermediates in the study of the reactivity is of primary importance to predict new catalysts, find universal descriptors, or attempt comparisons with experiments. The thermodynamic stability of the relevant reaction intermediates and the catalytic implications are also discussed.

2 Computational details

The calculations have been done within the framework of density functional theory (DFT) as implemented in the VASP package.[39–42] The PBE parametrization of the exchange and correlation functional was used.[43] To consider the self-interaction error inherent to standard GGA functionals, we adopted the DFT+U approach.[44,45] PBE + U allows one to reproduce with acceptable accuracy the Gibbs free energies of water splitting intermediates computed at the PBE0 level (hybrid functional) for a wide series of SACs embedded in a carbon-based support with a similar local coordination to that of the COF investigated in this work.[46] The working U-correction term is reported in Table 1 and its origin has been discussed elsewhere.[46,47] The core electrons were treated with the Projector Augmented Method (PAW) and the valence electrons were expanded on a set of plane waves with a kinetic energy cutoff of 400 eV.[48,49] The threshold criteria for the convergence of electronic energies of forces of the ions were set to 10^{-5} eV and 10^{-2} eV Å^{-1} respectively. Dispersion forces have been included by means of the Grimme's D3 scheme.[50] The sampling of the reciprocal space was reduced to the gamma point because of the large cell size.[51] The unit cell of the COF matrix was fully relaxed. After including the metal atom, as well as for each reaction intermediate, the atomic coordinates of were fully reoptimized keeping fixed the lattice constants. This represents a reasonable approximation, since it usually leads to negligible errors.[47]

Table 1 Adsorption energy, atomic magnetization, and Bader charge of TMs adsorbed in the cavity of COF. The U parameter used in the calculations is also reported

TM	E_{ad}/eV	Magnetization/μ_B	$q(M)/\lvert e\rvert$	$U^{46,47,70}$/eV
Ti	−10.46	1.05	1.85	2.58
V	−10.13	2.37	1.51	2.72
Cr	−9.36	3.55	1.32	2.93
Mn	−8.24	3.44	1.36	3.06
Fe	−8.93	2.02	1.04	3.29
Co	−9.27	1.05	1.09	3.42
Ni	−9.46	0.00	0.98	3.40
Nb	−11.12	1.28	1.89	2.02
Mo	−9.27	2.86	1.61	2.30
Ru	−9.51	1.66	1.16	2.79
Rh	−9.26	0.90	1.03	3.04
Pd	−8.39	0.00	0.75	3.33
Ta	−11.98	1.04	2.00	1.87
W	−11.17	2.33	1.77	2.08
Os	−9.98	1.54	1.05	2.51
Ir	−10.34	0.73	0.90	2.74
Pt	−10.58	0.00	0.79	2.95

The reaction Gibbs free energies were obtained by adopting the seminal thermochemistry approach of Norskov and co-workers:[52–56]

$$\Delta G = \Delta H - T\Delta S + \Delta E_{ZPE}$$

ΔH is obtained from calculated DFT energies. The entropic contribution at 298 K of gas phase species ($T\Delta S$) is taken from International Tables and that of solid-state systems is neglected.[52,53,56] This assumption can be improved by estimating the entropy of adsorbates by means of the partition function formalism. However, this contribution is often small (about 0.1–0.2 eV), and therefore can be neglected.[37] ΔE_{ZPE} is the zero-point energy correction that was evaluated in a

harmonic fashion by allowing to vibrate all the atoms of the reaction intermediates and the metal.[37] Tables S1 and S2 (ESI†) report the main working quantities adopted.

Of course, other effects can be relevant in modeling the reaction, in particular pH-dependence and solvation effects should be considered to provide quantitative predictions.[57–65] Nevertheless, the purpose of this work is to assess the overall ability of SACs stabilized at COF to catalyze HER and OER and to analyze the similarities or differences that TM atoms embedded in COFs present compared to other supporting matrices with similar local structure, such as N-doped graphene or carbon nitride. In this respect, models that do not include solvation effects can provide a first assessment. The role of the solvent will be specifically addressed in future studies.

3 Results and discussion

The reference COF material is made by a 2D periodic arrangement of building blocks and stacking of different nanosheets along the third dimension, similarly to what occurs in graphene-based and carbon nitride materials. A common approximation is to model the systems with a single nanosheet.[66,67] The optimized lattice parameters of the COF structure are a = 20.318 Å and b = 20.318 Å. The TM atoms are stably embedded in the matrix with a square planar coordination, Fig. 1. The adsorption of the metal atom in the cavity leads to SACs with very strong binding energies, see Table 1. The atomic-like character of the TM atoms is shown by the net magnetization on several TM atoms, Table 1.[68] We observe that the binding energies of the TM atoms are larger, in absolute value, than those of the same species on N-doped graphene or carbon nitride.[14,46] For instance, Co has a binding energy to COF of −9.27 eV, while it binds to N–Gr and C_3N_4 by −7.79 eV and −3.34 eV, respectively. Similarly, the binding energy of Pt is −10.58 eV in COF, to be compared with −7.99 eV (N–Gr) and −2.79 eV (C_3N_4). Table S3 (ESI†) reports the metal binding energies in the COF compared with that of other carbon-based materials. This suggests that COFs may be good candidates in stabilizing the TM atoms and avoid diffusion and sintering. On the other side, this result can imply a lower reactivity of the SAC towards adsorbates, based on the bond order conservation principle.[69]

3.1 Hydrogen evolution

To study the activity of SACs@COF in HER we adsorbed a hydrogen atom on the TM active site. Fig. 2 shows an example of local geometry of the adducts, and Table 2 reports the calculated Gibbs free energies and structural parameters. The high stability of the SACs discussed above often reflects in a moderate reactivity towards hydrogen as shown by the fact that most of the SACs considered exhibit positive free energies of adsorption. Of course, there are differences, and the nature of the TM has a primary effect. For instance, among 3d elements only Ti can form H* species with a negative ΔG. Some atoms, see *e.g.* Mo@COF and Ru@COF, bind H* with $\Delta G \sim 0$ eV, which is close to the ideal value according to the classical Norskov's model (the catalyst binds H not too strongly nor too weakly). Heavy metals such as Rh@COF (−0.32 eV) and Ir@COF (−0.61 eV) bind H* more strongly and could also exhibit some activity according to Norskov's model. On the contrary, noble metal atoms such as Ni, Pd, and Pt are expected to be inert, since the $\Delta G > 1.5$ eV is very far from the ideal condition for high reactivity ($\Delta G \sim 0$ eV). Overall, Fig. S1 (ESI†) shows a general trend where 4d and 5d TMs are more reactive than 3d ones, forming more stable H* species.

The picture becomes more interesting when one considers two hydrogen atoms binding simultaneously to the TM. Recently we have shown that these are stable species, with strong analogies with coordination chemistry compounds, and that they need to be accounted for when SACs are involved in HER.[13,38] The formation of dihydrogen complexes can be considered the first step of hydrogenation reactions, or, *viceversa*, the last before step before the release of molecular hydrogen to the gas-phase in HER. In a dihydrogen complex (H_2*), the H–H bond length is slightly elongated with respect that of the free H_2 molecule, while in dihydride complexes (H*H*) the H–H bond is completely broken,[71–74] Table 2. Ti@COF, V@COF, and W@COF form dihydrogen complexes nearly thermoneutral with respect to the H_2 molecule and the free catalyst, with ΔG = −0.03 eV, 0.12 eV, and −0.13 eV respectively. Cr@COF and Mn@COF can potentially form a dihydrogen complex, which is however a local minimum along the potential energy surface, given the positive Gibbs free energies. In some cases, see W@COF and Ta@COF, the complex displays dihydride character (H*H*), Table 2.[71–74] In particular, the formation of H*H* on W@COF is nearly thermoneutral with respect to the free H_2 molecule. Finally, there are SACs that do not form dihydrogen complexes.

The importance to consider all the intermediates, including the double hydrogen complexes, to predict the catalytic activity of SACs becomes apparent looking at the case of Mo@COF.

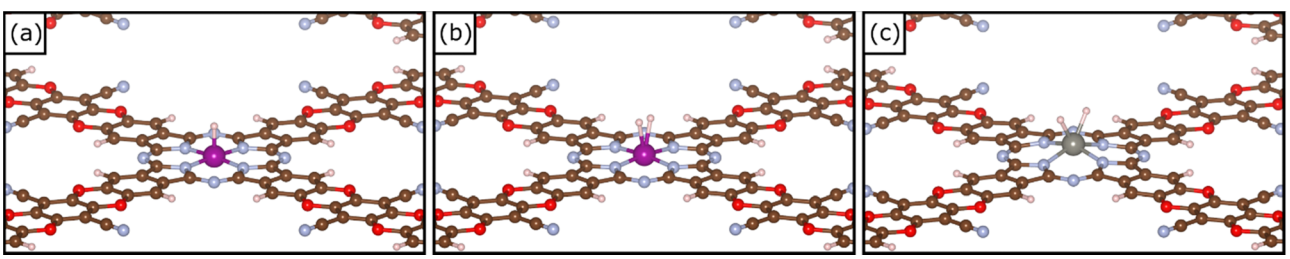

Fig. 2 (a) Example of local geometry of H*, (b) example of local geometry of a dihydrogen complex H_2* and (c) example of local geometry of a dihydride complex H*H* on TM@COF.

Table 2 Gibbs free energies of H* (ΔG_H) and H_2*/H*H* (ΔG_{H_2}) intermediates for HER on TM@COF and H–H and TM–H distances

TM	ΔG_H/eV	d_{TM-H}/Å	ΔG_{H2}/eV	d_{H-H}/Å	d_{TM-H}/Å
Ti	−0.10	1.71	−0.03	0.78	2.04
V	0.44	1.67	0.12	0.78	1.99
Cr	0.91	1.61	1.59	0.82	1.77
Mn	1.15	1.53	1.51	0.80	1.79
Fe	1.14	1.47	—	—	—
Co	0.77	1.41	—	—	—
Ni	1.73	1.40	—	—	—
Nb	−0.65	1.80	0.06	0.82	2.02
Mo	−0.03	1.70	0.57	0.88	1.90
Ru	0.01	1.59	0.34	0.75	2.82
Rh	−0.32	1.50	0.30	0.76	2.33
Pd	2.16	1.83	—	—	—
Ta	−0.76	1.76	−0.43	1.88	1.77
W	−0.47	1.70	−0.13	1.77	1.71
Os	−0.31	1.60	0.35	0.75	3.15
Ir	−0.61	1.53	0.49	0.77	2.18
Pt	1.92	1.61	—	—	—

If one considers the formation of the H* intermediate only (classical model), then the catalyst is predicted to be ideal ($\Delta G \sim 0$ eV); but if one considers also the formation of the H_2* complex, this is predicted to be a poor catalyst due to the positive free adsorption energy ($\Delta G = 0.57$ eV, Table 2). This means that the reaction implies an additional step, which is usually neglected if the analysis is limited to the single H adsorption.

Fig. 3 shows the calculated Gibbs free energies of single hydrogen, H*, and double hydrogen, H_2*/H*H*, intermediates, where one can observe that Ti@COF and Ru@COF bind the intermediates nearly ideally ($\Delta G \sim 0$ eV). These systems could potentially have a good activity in the HER. Also, we checked for a possible relation between the free energy of adsorption of H* and that of H_2*/H*H*, but we did not find clear correlations, Fig. S2 (ESI†). This shows that it is not easy to find scaling relationships for SACs involved in HER due to their complex chemistry.[14,38]

3.2 Oxygen evolution

We now discuss the reactivity of TM@COF in the Oxygen Evolution Reaction (OER). On metal electrodes the reaction is commonly assumed to proceed *via* consecutive reactions involving one electron transfer at the time, as reported below.

$$* + H_2O \rightarrow OH^* + H^+ + e^- \quad (1)$$

$$OH^* \rightarrow O^* + H^+ + e^- \quad (2)$$

$$O^* + H_2O \rightarrow OOH^* + H^+ + e^- \quad (3)$$

$$OOH^* \rightarrow O_2 + * + H^+ + e^- \quad (4)$$

Table 3 reports the calculated Gibbs free energies for each of these intermediates that we classify as "conventional" since these are the species that are usually taken into account in the discussion of the mechanism of the OER. Starting from the initial step, OH* formation, eqn (1), we observe that the nature of the metal largely affects the stability of the species. For instance, Ti@COF and W@COF bind OH* strongly. Ir@COF, Rh@COF, Mn@COF, Fe@COF, and Co@COF bind OH* with a free energy ~1.2 eV, the ideal value for an OER catalyst. Some metals, Ni@COF, Pd@COF, and Pt@COF, are very weakly reactive due to the too large and positive ΔG. A similar result is obtained when looking at the O* intermediate, eqn (2), where we observe a quite broad scenario, ranging from very reactive species, such as Ti@COF, and W@COF to rather inert ones such as Ni@COF, Pd@COF, Pt@COF.

The next intermediate is OOH*, eqn (3). For some systems, such as Ti@COF and V@COF, we did not detect its formation although both OH* and O* species are quite stable. Interestingly, we detected the formation of a related species where the O–OH bond is completely broken, resulting in an OH* O* intermediate (Table 3) bound to the catalyst with both oxygen atoms. The formation of such unconventional intermediate has been previously predicted on other SACs supported on carbon-based materials.[14]

The role of unconventional intermediates for the OER on SACs has been emphasized only recently, and their formation opens interestingly new routes for the catalyst optimization. Furthermore, they are indicative of how complex is the chemistry of SACs.[13,14] In general, once OH* adsorbs to the catalyst,

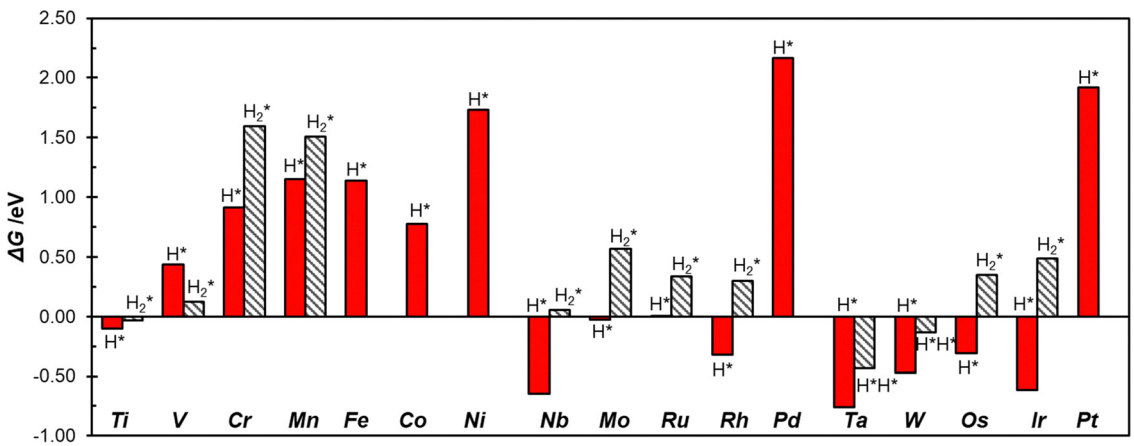

Fig. 3 Gibbs free energies of H* and H_2*/H*H* intermediates adsorbed at TM@COF SACs.

Table 3 Gibbs energies of conventional (OH*, O* and OOH*) and unconventional (OH*OH*, OH*O* and dioxygen complexes, η^1 and η^2) intermediates for OER on TM@COF

M	ΔG_{OH}/eV	ΔG_O/eV	ΔG_{OOH}/eV	ΔG_{OHOH}/eV	ΔG_{OHO}/eV	ΔG_{η_1}/eV	ΔG_{η_2}/eV
Ti	−1.51	−1.46	—	−1.02	0.81	1.27	1.25
V	−0.60	−0.76	—	0.86	1.47	—	—
Cr	1.62	1.89	4.88	3.11	4.46	4.53	4.87
Mn	1.27	2.15	4.96	3.16	4.96	4.71	4.76
Fe	1.54	2.53	4.36	3.72	5.47	5.12	—
Co	1.70	3.44	4.75	5.00	6.65	4.99	—
Ni	2.40	4.60	5.45	—	—	—	—
Nb	−2.03	2.30	—	−1.78	−1.97	0.96	−0.02
Mo	−0.05	−0.86	3.09	0.41	0.54	3.69	0.76
Ru	0.62	1.31	3.79	2.91	4.29	4.38	5.73
Rh	1.14	2.97	4.49	4.24	5.88	4.63	7.76
Pd	2.73	4.94	—	—	—	—	—
Ta	−1.92	−2.28	—	−2.23	−2.08	0.46	−0.19
W	−0.81	−1.68	—	−0.48	−0.45	1.95	−0.43
Os	0.49	0.90	3.64	2.38	3.05	4.24	4.10
Ir	1.04	2.16	4.38	3.79	5.20	4.61	6.83
Pt	2.63	4.84	—	—	—	—	—

the system can bind another water molecule, resulting in the formation of a OH*OH* intermediate:[13]

$$OH^* + H_2O \rightarrow OH^*OH^* + H^+ + e^- \quad (5)$$

This species is competitive with O*, since it implies the release of two electrons starting from the clean catalyst. Similarly, the OH*O* species discussed above is competitive with the OOH* intermediate:

$$OH^*OH^* \rightarrow OH^*O + H^+ + e^- \quad (6)$$

Finally, before the release of the free oxygen molecule to the gas-phase, SACs can form stable peroxo or superoxo complexes with O_2:

$$OH^*O^* \rightarrow O_2^* + H^+ + e^- \quad (7)$$

In these dioxygen species, if the O–O bond distance is only slightly elongated from that of the free O_2 molecule (1.25 Å) the system can be classified as a superoxo complex (η^1) (1.25–1.35 Å); when the O–O bond length is larger (1.35–1.45 Å), the system is classified as a peroxo complex. Eventually, in the case of a complete O–O bond breaking, one is in the presence of a dioxo complex, O*O*. In these last two cases the TM is bound *via* two M–O bonds in to the intermediate (η^2). Fig. 4 reports some examples of the structure of different oxygenate intermediates adsorbed on SACs@COF. It must be mentioned that the picture can be even more complex if one considers that intermediates binding with two ligands can be attached to the metal both in *syn-* and *anti-* configurations.[14] However, the latter case will unlikely release the product. We decided to restrict the present study to *syn-* intermediates since the scope of this work is to investigate the reactivity of SACs supported on a COF.

The OH*OH* intermediate is more stable than the O* only in the case of Ta@COF, thus, this is the species that is expected to form. The remaining metals bind O* more strongly than OH*OH*, so that the latter is only a local minimum along the potential energy surface.

In the next step, the OH*O* intermediate is the global minimum for several metals such as Cr@COF, Mn@COF, Mo@COF, and Os@COF, indicating that these systems are not expected to form the "conventional" OOH* species. Interestingly, Ta@COF and W@COF form only the OH*O* complex, showing that for these two systems the conventional path is clearly prevented.

Several systems form a stable dioxygen complex before they release O_2 to the gas-phase. Table S4 (ESI†) reports the calculated O–O bond distances. In particular, a superoxo complex, η^1, is found on Cr@COF, Mn@COF, Fe@COF, Co@COF, Ru@COF, Rh@COF and Ir@COF. On the contrary, Ti@COF leads to a peroxo adduct, η^2. On Nb@COF, Mo@COF, Ta@COF, W@COF and Os@COF the O–O bond is completely broken, leading to a O*O* dioxocomplex. Interestingly, the Ni-triad, Ni@COF, Pd@COF, and Pt@COF, is unreactive. In particular, Ni forms weakly bounds conventional intermediates only, and Pd@COF, and Pt@COF are not able to bind neither OOH* nor OH*O* species.

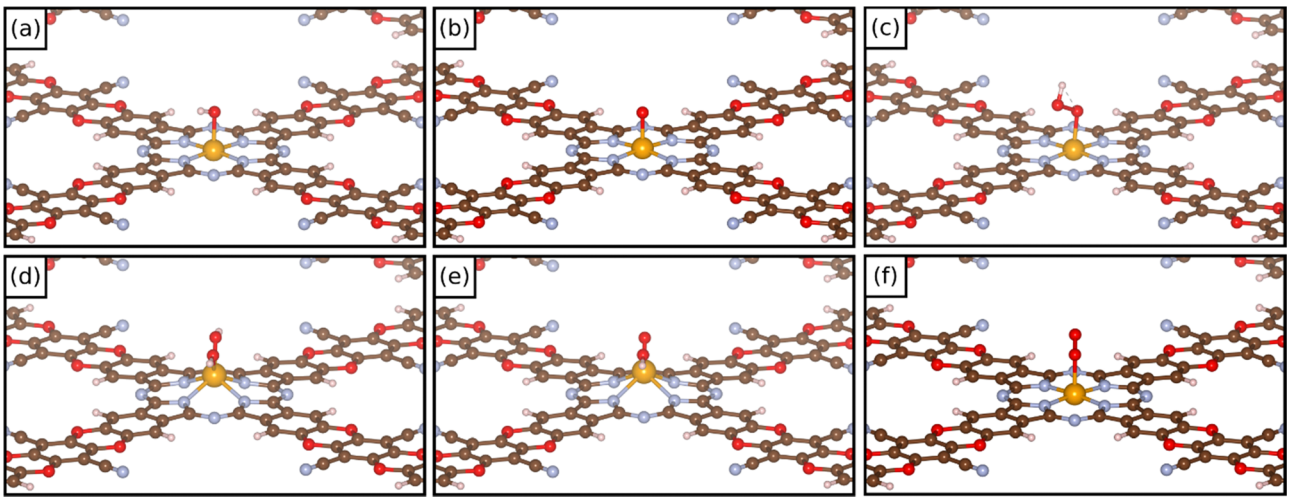

Fig. 4 Examples of the structure of (a) OH*, (b) O*, (c) OOH*, (d) OH*OH*, (e) OH*O*, and (f) O_2* intermediates on COF-based SACs.

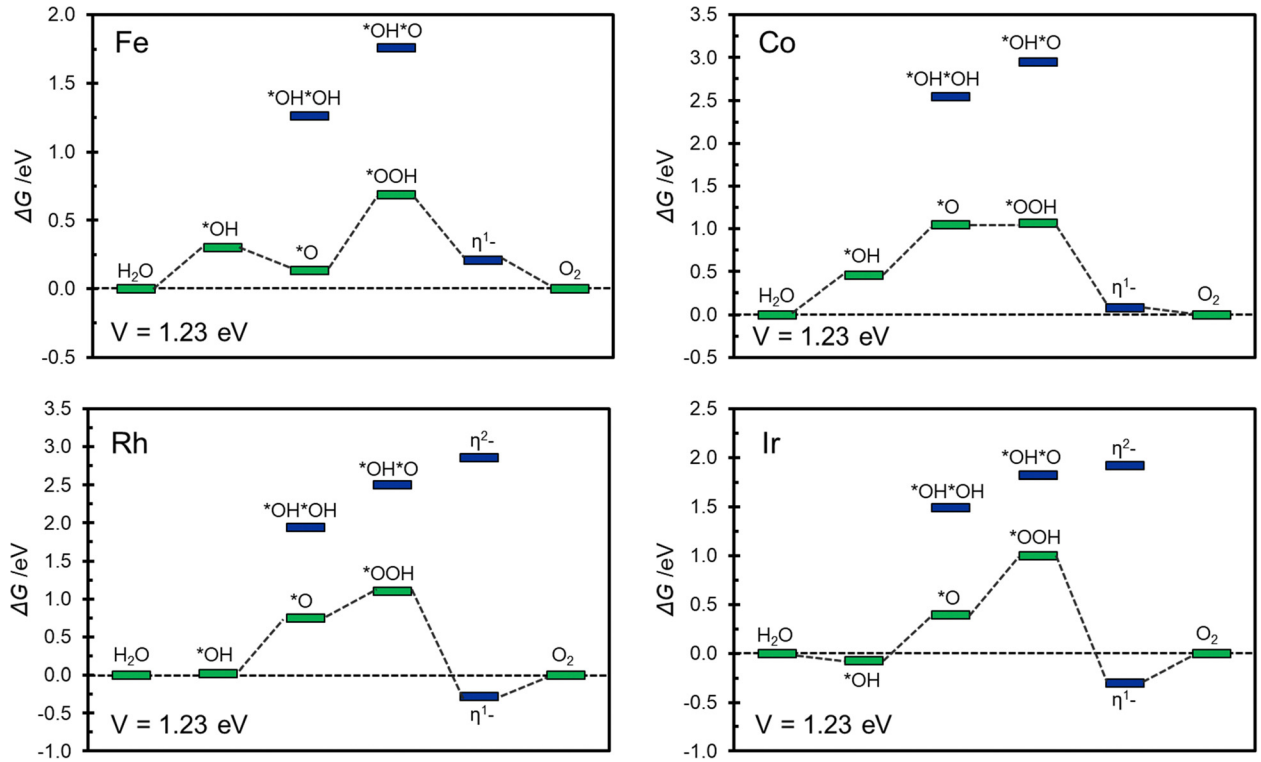

Fig. 5 Gibbs free energy profile at V = 1.23 V for Fe@COF, Co@COF, Rh@COF, and Ir@COF SACs. In green and blue are reported conventional and unconventional intermediates respectively.

These results show that most SACs involve the formation of at least one unconventional intermediate. In this respect, the classical path for OER is not the preferred one except for Fe@COF, Co@COF, and Ni@COF, Table 3. This result is consistent with previous calculations indicating that on SACs the OER follows a path characterized by the formation of unconventional intermediates, typical of coordination compounds.[14] We also observe that the formation of unconventional intermediates can cause some protrusion of about 0.1 Å of the metal atom from the plane of the 2D COF to stabilize the adduct.[14]

Of the relatively large number of systems considered, only Fe@COF, Co@COF, Rh@COF and Ir@COF seem to exhibit interesting catalytic activity associated to a relatively small overpotential, around 0.5–0.6 eV. This is similar to the best overpotential expected with conventional catalysts.[56,75] Fig. 5 shows the corresponding Gibbs free energy profiles where it is possible to appreciate the most likely reaction path. The Gibbs free energy profiles are reported assuming to work at an applied voltage of 1.23 V, corresponding to the working condition of an ideal catalyst. This allows to gain some insight about the presence and extent of overpotentials as well as on the nature of the limiting potential of the reaction.[56,75]

Conclusions

In this work we performed a computational study of a set of single atom catalysts consisting of transition metal atoms embedded in a recently prepared Covalent Organic Framework. The catalytic activity was investigated for the two semi-reactions of water splitting, *i.e.* the Hydrogen Evolution and the Oxygen Evolution Reactions.

The TM atoms are strongly bound to the COF structures, with positive consequences on the expected thermodynamic stability of the catalysts but the potentially negative effects on their reactivity (more stable species are usually less reactive). In this respect, the nature of the metal is of primary importance to determine the final reactivity and the stability of the reaction intermediates. Out of 17 SACs considered, four are predicted to be rather good for the HER (Ti@COF, W@COF, Ru@COF, Rh@COF); another four exhibit appreciable activities in OER (Fe@COF, Co@COF, Ir@COF, and Rh@COF). From this it emerges that only Rh@COF is, in principle, a good catalyst for both HER and OER. Future work is planned to verify if these conclusions hold true also for the same systems in a water environment.

The other relevant conclusion is that SACs@COF form several unconventional intermediates in both HER and OER and that these species can be more stable than the classical HER and OER adducts. This derives from the fact that SACs are analogs of coordination chemistry compounds and as such they exhibit a rich and complex chemistry. The formation of non-classical intermediates can affect both the thermodynamics and the kinetics of the HER and OER processes. Neglecting the formation of these species in the computational screening of new catalytic systems can result in totally unreliable predictions. Further work will be dedicated in the future to

the investigation of more complex *syn*- and *anti*-adsorbates for relevant electrochemical reactions, as well as the role of solvation.

Author contributions

Dr Ilaria Barlocco: data simulation, revision and discussion. Dr Giovanni Di Liberto: supervision, revision and discussion. Prof. Gianfranco Pacchioni: supervision, funding acquisition, revision and discussion. The manuscript was written through contributions of all authors.

Conflicts of interest

The authors declare no conflict of interest.

Acknowledgements

We thank Livia Giordano for useful discussions. Access to the CINECA supercomputing resources was granted *via* ISCRAB. We also thank the COST Action 18234 supported by COST (European Cooperation in Science and Technology).

References

1 A. Wang, J. Li and T. Zhang, *Nat. Rev. Chem.*, 2018, **2**, 65–81.
2 S. K. Kaiser, Z. Chen, D. Faust Akl, S. Mitchell and J. Pérez-Ramírez, *Chem. Rev.*, 2020, **120**, 11703–11809.
3 M. A. Bajada, J. Sanjosé-Orduna, G. Di Liberto, S. Tosoni, G. Pacchioni, T. Noël and G. Vilé, *Chem. Soc. Rev.*, 2022, **51**, 3898–3925.
4 H. Xu, Y. Zhao, Q. Wang, G. He and H. Chen, *Coord. Chem. Rev.*, 2022, **451**, 214261.
5 S. Tosoni, G. Di Liberto, I. Matanovic and G. Pacchioni, *J. Power Sources*, 2023, **556**, 232492.
6 M. B. Gawande, P. Fornasiero and R. Zbořil, *ACS Catal.*, 2020, **10**, 2231–2259.
7 G. Di Liberto, L. A. Cipriano and G. Pacchioni, *ChemCatChem*, 2022, **14**, e202200611.
8 X. Li, H. Rong, J. Zhang, D. Wang and Y. Li, *Nano Res.*, 2020, **13**, 1842–1855.
9 C. Ling, Y. Ouyang, Q. Li, X. Bai, X. Mao, A. Du and J. Wang, *Small Methods*, 2019, **3**, 1800376.
10 C. Copéret, A. Comas-Vives, M. P. Conley, D. P. Estes, A. Fedorov, V. Mougel, H. Nagae, F. Núñez-Zarur and P. A. Zhizhko, *Chem. Rev.*, 2016, **116**, 323–421.
11 J. Wang, C. Y. Fan, Q. Sun, K. Reuter, K. Jacobi, M. Scheffler and G. Ertl, *Angew. Chem., Int. Ed.*, 2003, **42**, 2151–2154.
12 C. Asokan, H. V. Thang, G. Pacchioni and P. Christopher, *Catal. Sci. Technol.*, 2020, **10**, 1597–1601.
13 L. Zhong and S. Li, *ACS Catal.*, 2020, **10**, 4313–4318.
14 I. Barlocco, L. A. Cipriano, G. Di Liberto and G. Pacchioni, *J. Catal.*, 2023, **417**, 351–359.
15 Z. Lin, M. Escudero-Escribano and J. Li, *J. Mater. Chem. A*, 2022, **10**, 5670–5672.
16 N. Cheng, S. Stambula, D. Wang, M. N. Banis, J. Liu, A. Riese, B. Xiao, R. Li, T.-K. Sham, L.-M. Liu, G. A. Botton and X. Sun, *Nat. Commun.*, 2016, **7**, 13638.
17 W. Qiao, W. Xu, X. Xu, L. Wu, S. Yan and D. Wang, *ACS Appl. Energy Mater.*, 2020, **3**, 2315–2322.
18 G. Vilé, G. Di Liberto, S. Tosoni, A. Sivo, V. Ruta, M. Nachtegaal, A. H. Clark, S. Agnoli, Y. Zou, A. Savateev, M. Antonietti and G. Pacchioni, *ACS Catal.*, 2022, **12**, 2947–2958.
19 G. Di Liberto, S. Tosoni, L. A. Cipriano and G. Pacchioni, *Acc. Mater. Res.*, 2022, **3**, 986–995.
20 D. Van Dao, L. A. Cipriano, G. Di Liberto, T. T. D. Nguyen, S.-W. Ki, H. Son, G.-C. Kim, K. H. Lee, J.-K. Yang, Y.-T. Yu, G. Pacchioni and I.-H. Lee, *J. Mater. Chem. A*, 2021, **9**, 22810–22819.
21 D. Van Dao, G. Di Liberto, H. Ko, J. Park, W. Wang, D. Shin, H. Son, Q. Van Le, T. Van Nguyen, V. Van Tan, G. Pacchioni and I.-H. Lee, *J. Mater. Chem. A*, 2022, **10**, 3330–3340.
22 Y. Chen, S. Ji, C. Chen, Q. Peng, D. Wang and Y. Li, *Joule*, 2018, **2**, 1242–1264.
23 H. Fei, J. Dong, D. Chen, T. Hu, X. Duan, I. Shakir, Y. Huang and X. Duan, *Chem. Soc. Rev.*, 2019, **48**, 5207–5241.
24 M. D. Hossain, Z. Liu, M. Zhuang, X. Yan, G.-L. Xu, C. A. Gadre, A. Tyagi, I. H. Abidi, C.-J. Sun, H. Wong, A. Guda, Y. Hao, X. Pan, K. Amine and Z. Luo, *Adv. Energy Mater.*, 2019, **9**, 1803689.
25 J. Deng, H. Li, J. Xiao, Y. Tu, D. Deng, H. Yang, H. Tian, J. Li, P. Ren and X. Bao, *Energy Environ. Sci.*, 2015, **8**, 1594–1601.
26 C. Lin, L. Zhang, Z. Zhao and Z. Xia, *Adv. Mater.*, 2017, **29**, 1606635.
27 Z. Li, N. Huang, K. H. Lee, Y. Feng, S. Tao, Q. Jiang, Y. Nagao, S. Irle and D. Jiang, *J. Am. Chem. Soc.*, 2018, **140**, 12374–12377.
28 C. A. Trickett, A. Helal, B. A. Al-Maythalony, Z. H. Yamani, K. E. Cordova and O. M. Yaghi, *Nat. Rev. Mater.*, 2017, **2**, 17045.
29 V. Hasija, S. Patial, P. Raizada, A. Aslam Parwaz Khan, A. M. Asiri, Q. Van Le, V.-H. Nguyen and P. Singh, *Coord. Chem. Rev.*, 2022, **452**, 214298.
30 Z. Meng, R. M. Stolz and K. A. Mirica, *J. Am. Chem. Soc.*, 2019, **141**, 11929–11937.
31 Y. Yue, P. Cai, K. Xu, H. Li, H. Chen, H.-C. Zhou and N. Huang, *J. Am. Chem. Soc.*, 2021, **143**, 18052–18060.
32 Q. Guan, G.-B. Wang, L.-L. Zhou, W.-Y. Li and Y.-B. Dong, *Nanoscale Adv.*, 2020, **2**, 3656–3733.
33 J. Wang, J. Wang, S. Qi and M. Zhao, *J. Phys. Chem. C*, 2020, **124**, 17675–17683.
34 J. Wang, Z. Zhang, Y. Li, Y. Qu, Y. Li, W. Li and M. Zhao, *ACS Appl. Mater. Interfaces*, 2022, **14**, 1024–1033.
35 M. Lu, M. Zhang, C. Liu, J. Liu, L. Shang, M. Wang, J. Chang, S. Li and Y. Lan, *Angew. Chem.*, 2021, **133**, 4914–4921.
36 J. P. Collman, R. R. Gagne, C. Reed, T. R. Halbert, G. Lang and W. T. Robinson, *J. Am. Chem. Soc.*, 1975, **97**, 1427–1439.
37 L. A. Cipriano, G. Di Liberto and G. Pacchioni, *ACS Catal.*, 2022, 11682–11691.
38 G. Di Liberto, L. A. Cipriano and G. Pacchioni, *J. Am. Chem. Soc.*, 2021, **143**, 20431–20441.

39 G. Kresse and J. Hafner, *Phys. Rev. B: Condens. Matter Mater. Phys.*, 1993, **47**, 558–561.
40 G. Kresse and J. Hafner, *Phys. Rev. B: Condens. Matter Mater. Phys.*, 1994, **49**, 14251–14269.
41 G. Kresse and J. Furthmüller, *Comput. Mater. Sci.*, 1996, **6**, 15–50.
42 G. Kresse and J. Furthmüller, *Phys. Rev. B: Condens. Matter Mater. Phys.*, 1996, **54**, 11169–11186.
43 J. P. Perdew, K. Burke and M. Ernzerhof, *Phys. Rev. Lett.*, 1996, **77**, 3865–3868.
44 S. L. Dudarev, G. A. Botton, S. Y. Savrasov, C. J. Humphreys and A. P. Sutton, *Phys. Rev. B: Condens. Matter Mater. Phys.*, 1998, **57**, 1505–1509.
45 S. L. Dudarev, G. A. Botton, S. Y. Savrasov, C. J. Humphreys and A. P. Sutton, *Phys. Rev. B: Condens. Matter Mater. Phys.*, 1998, **57**, 1505–1509.
46 I. Barlocco, L. A. Cipriano, G. Di Liberto and G. Pacchioni, *Adv. Theory Simul.*, 2022, 2200513.
47 G. Di Liberto, L. A. Cipriano and G. Pacchioni, *ACS Catal.*, 2022, 5846–5856.
48 P. E. Blöchl, *Phys. Rev. B: Condens. Matter Mater. Phys.*, 1994, **50**, 17953–17979.
49 G. Kresse and D. Joubert, *Phys. Rev. B: Condens. Matter Mater. Phys.*, 1999, **59**, 1758–1775.
50 S. Grimme, J. Antony, S. Ehrlich and H. Krieg, *J. Chem. Phys.*, 2010, **132**, 154104.
51 H. J. Monkhorst and J. D. Pack, *Phys. Rev. B: Condens. Matter Mater. Phys.*, 1976, **13**, 5188–5192.
52 J. K. Nørskov, T. Bligaard, A. Logadottir, J. R. Kitchin, J. G. Chen, S. Pandelov and U. Stimming, *J. Electrochem. Soc.*, 2005, **152**, J23.
53 J. K. Nørskov, T. Bligaard, J. Rossmeisl and C. H. Christensen, *Nat. Chem.*, 2009, **1**, 37–46.
54 J. K. Norskov and C. H. Christensen, *Science*, 2006, **312**, 1322 LP–1323.
55 Y. Sha, T. H. Yu, B. V. Merinov, P. Shirvanian and W. A. Goddard, *J. Phys. Chem. Lett.*, 2011, **2**, 572–576.
56 J. K. Nørskov, J. Rossmeisl, A. Logadottir, L. Lindqvist, J. R. Kitchin, T. Bligaard and H. Jónsson, *J. Phys. Chem. B*, 2004, **108**, 17886–17892.
57 Z.-D. He, S. Hanselman, Y.-X. Chen, M. T. M. Koper and F. Calle-Vallejo, *J. Phys. Chem. Lett.*, 2017, **8**, 2243–2246.
58 F. Calle-Vallejo, R. F. de Morais, F. Illas, D. Loffreda and P. Sautet, *J. Phys. Chem. C*, 2019, **123**, 5578–5582.
59 P. Gono, F. Ambrosio and A. Pasquarello, *J. Phys. Chem. C*, 2019, **123**, 18467–18474.
60 A. Bouzid, P. Gono and A. Pasquarello, *J. Catal.*, 2019, **375**, 135–139.
61 G. Di Liberto, F. Maleki and G. Pacchioni, *J. Phys. Chem. C*, 2022, **126**, 10216–10223.
62 L. Giordano, B. Han, M. Risch, W. T. Hong, R. R. Rao, K. A. Stoerzinger and Y. Shao-Horn, *Catal. Today*, 2016, **262**, 2–10.
63 G. Di Liberto and L. Giordano, *Electrochem. Sci. Adv.*, 2023, e2100204.
64 S. Rojas-Carbonell, K. Artyushkova, A. Serov, C. Santoro, I. Matanovic and P. Atanassov, *ACS Catal.*, 2018, **8**, 3041–3053.
65 F. Maleki, G. Di Liberto and G. Pacchioni, *ACS Appl. Mater. Interfaces*, 2023, **15**, 11216–11224.
66 V. Dao, L. A. Cipriano, S.-W. Ki, S. Yadav, W. Wang, G. Di Liberto, K. Chen, H. Son, J.-K. Yang, G. Pacchioni and I.-H. Lee, *Appl. Catal., B*, 2023, **330**, 122586.
67 J. Wang, Z. Zhang, Y. Li, Y. Qu, Y. Li, W. Li and M. Zhao, *ACS Appl. Mater. Interfaces*, 2022, **14**, 1024–1033.
68 M. T. Greiner, T. E. Jones, S. Beeg, L. Zwiener, M. Scherzer, F. Girgsdies, S. Piccinin, M. Armbrüster, A. Knop-Gericke and R. Schlögl, *Nat. Chem.*, 2018, **10**, 1008–1015.
69 E. Shustorovich, *Surf. Sci. Rep.*, 1986, **6**, 1–63.
70 I. V. Solovyev, P. H. Dederichs and V. I. Anisimov, *Phys. Rev. B: Condens. Matter Mater. Phys.*, 1994, **50**, 16861–16871.
71 G. J. Kubas, *Acc. Chem. Res.*, 1988, **21**, 120–128.
72 G. J. Kubas, *Chem. Rev.*, 2007, **107**, 4152–4205.
73 R. H. Crabtree, *Acc. Chem. Res.*, 1990, **23**, 95–101.
74 R. H. Crabtree, *Chem. Rev.*, 2016, **116**, 8750–8769.
75 A. Kulkarni, S. Siahrostami, A. Patel and J. K. Nørskov, *Chem. Rev.*, 2018, **118**, 2302–2312.